Chemical Geology
March 2021, Volume 563, Pages 120050 (8p.)
https://doi.org/10.1016/j.chemgeo.2020.120050
https://archimer.ifremer.fr/doc/00668/77998/

The Nickel isotope composition of the authigenic sink and the diagenetic flux in modern oceans

Gueguen Bleuenn [1, 2, *], Rouxel Olivier [3]

[1] CNRS, Univ Brest, UMR 6538 Laboratoire Géosciences Océan, F-29280 Plouzané, France
[2] CNRS, Univ Brest, UMS 3113, F- 29280 Plouzané, France
[3] IFREMER, Centre de Brest, Unité Géosciences Marines, F-29280 Plouzané, France

* Corresponding author : Bleuenn Gueguen, email address : bleuenn.gueguen@univ-brest.fr

Abstract :

We investigated Ni isotope composition in a stratigraphic sequence of pelagic clays collected during ODP core leg 185 on site 1149 in Western Pacific Ocean near the Izu-Bonin subduction trench in order to determine the Ni isotope composition of the authigenic Mn-oxides sink and evaluate the Ni isotope composition of the diagenetic input flux. This predominant oxic sink likely controls the Ni isotope budget in modern oceans. The sequence presented here is a 170 m-thick sequence of pelagic sediments deposited on some of the oldest oceanic crust of the seafloor, and the base was dated at 104 Ma. Nickel isotope values (δ60/58Ni relative to NIST SRM 986) vary in the range of 0.04 ± 0.04 to 1.03 ± 0.03‰. There is a trend between depth in the stratigraphic sequence and increasing Mn/Fe, Mn/Al, higher Ni concentration and heavier Ni isotope values. This trend is accounted for by authigenic Mn-oxyhdroxides precipitation in the sediment and scavenging of dissolved metals in the sediment porewaters. This indicates that authigenic oxide minerals in deep-sea pelagic clays are a relevant sink for Ni in modern oceans. Results enable us to determine the authigenic oxic output flux of 3.58 × 108 mol/yr of Ni with a Ni isotope composition of 1.2‰, this oxic output is ~0.4‰ lighter than the oxic output flux in FeMn crusts and nodules. This study shows that Ni isotope variations along the stratigraphic sequence could be the result of mixing between a pure pelagic clays end-member at ~0.1‰ and a pure Mn-oxyhydroxides end-member at ~1.2‰. We suggest that to keep the system at steady-state conditions the oxic output flux is compensated for by a diagenetic input flux of 3.7 × 108 mol/yr which is characterized by a highly fractionated Ni isotope composition of ~2.9‰.

Introduction

It has long been demonstrated that deep-sea pelagic clays can display significant enrichment in transition metals in comparison to lithogenic and terrigenous sediments (Goldberg and Arrhenius, 1958; Boström and Peterson, 1966; Boström et al., 1969; Krishnaswami, 1976; Kadko, 1985; Leinen, 1987; Glasby, 1991; Kyte et al., 1993). The mechanism of trace metals scavenging by authigenic Mn oxides with subsequent burial in sediments has long been identified as an important output to the oceans, but estimating the global Fe-Mn oxide sink of a range of trace metals remains difficult. Previous work used Fe-Mn crust and Mn-nodules to estimate the global authigenic sink of a range of elements that are associated with Mn (Scott and Lyons, 2012; Gall et al., 2013; Hannington, 2013; Cameron and Vance, 2014; Little et al., 2014; Little et al., 2015). Owing to the progress in our understanding of metal isotope systematics and analytical developments (Albarède and Beard, 2004; Schauble, 2004; Anbar and Rouxel, 2007), as well as the fact that contrasted isotope fractionation takes place between oxic and anoxic seawater sinks, metal isotopes are now being used as powerful proxies of biogeochemical processes affecting the Earth's surface and subsurface. A popular example is that of Mo isotopes which were used as redox tracers in ancient and modern oceans. Molybdenum isotopes budget in seawater is controlled by the relative importance of oxic versus anoxic sink fluxes in the oceans and they likely varied through geological time (Archer and Vance, 2008; Goldberg et al., 2009; Nägler et al., 2011; Reinhard et al., 2013; Wille et al., 2013).

More recently, Ni isotopes were investigated in hydrogenetic ferromanganese crusts deposits as proxies of deep seawater Ni isotope composition through the Cenozoic (Gall et al., 2013; Gueguen et al., 2016). Nickel is essentially supplied to the oceans through riverine inputs while precipitation of Ni in authigenic Mn-oxides phases present in metalliferous deposits and pelagic clays removes Ni from seawater. Using the Ni isotope composition of hydrogenetic Fe-Mn crusts as an estimate of the authigenic Mn-oxides sink, the Ni isotope

composition measured in rivers and the Ni isotope composition of seawater, (Cameron and Vance, 2014) show an imbalance in the oceanic Ni isotope budget in modern oceans whereby seawater Ni isotopes are heavier than Ni isotopes in rivers while hydrogenetic Fe-Mn crusts are similar or heavier than seawater (Cameron and Vance, 2014; Vance et al., 2016; Takano et al., 2017; Wang et al., 2019). Vance et al. (2016) investigated the Ni isotope composition of Black Sea seawater samples and sediments to explore the possibility of a light Ni isotope input from sulfides. Results obtained from organic-rich sediments from the Peru margin show that this sink is not significant for Ni, and thus could not solve the imbalance of the Ni isotope budget (Ciscato et al., 2018). More recently, Little et al. (2020) investigated the Ni isotope composition of metalliferous deposits from the MANOP site in the Eastern Pacific Ocean. In this study, they show that an isotopically heavy (~3 ‰) Ni benthic input flux could balance the marine Ni isotope budget.

These studies emphasized the great importance of the oxic Ni output flux and in particular the role of Mn and diagenetic fluxes in the Ni biogeochemical cycling. However, the Ni isotope composition of authigenic phases in modern pelagic clays (the oxic sink) *sensu-stricto* has been documented only on a few samples (Gueguen et al., 2013). In order to untangle this uncertainty and to refine the Ni isotope mass balance budget, we aim this study to re-estimating the authigenic Ni sink flux by determining the long-term output flux of Ni and its isotopes in pelagic sediment that cannot be assessed by surficial materials such as nodules and Fe-Mn crusts only. Here, we present results of Ni isotope composition measured along a complete section of deep-sea pelagic clays from the ODP site 1149 in the Western Pacific.

2. Sample description and methods

Pelagic clay sediments were recovered from an ODP core at site 1149 (hole 1149A) in the Western Pacific Ocean off Izu-Bonin Trench during ODP Expedition 185 onboard the R/V Joides Resolution ~100 km east of the Izu-Bonin trench. (Figure 1). The whole stratigraphic sequence of pelagic clay sediments from the ODP core at site 1149 (hole 1149A) in the Western Pacific Ocean off Izu-Bonin Trench consists of four different units (Figure 2). Ages were determined by biochronology and paleomagnetism (Plank et al., 2000; Bartolini and Larson, 2001; Ludden et al., 2006). Unit I corresponds to the first 118 meters of sediments and it is composed of biogenic silica-bearing clays and several ash layers, and the unit represents a geological period of 6.5 Ma. Sediments from this uppermost unit were deposited below the CCD at water depths of ~6000 m and they are composed of clays, silts, several volcanic ashes layers which are probably the result of volcanic eruptions in the Izu-Bonin-Mariana arc, biogenic opaline silica and siliceous microfossils like radiolarians, diatoms and silicoflagellates. Accumulation rates of sediment are between 7 and 13 m/Ma. Unit II is a condensed sequence (from 6.5 to 104 Ma) of pelagic brown clays deposited on a thickness of 61 meters, thus sedimentation rates are very low: < 2 m/Ma. Siliceous microfossils are absent from this unit. Finally, the lowermost part of the sedimentary sequence (Units III and IV) is composed of a 229 meters-thick unit of hard radiolarian cherts (corresponding to a period of deposition of 13 Ma). These cherts correspond to siliceous pelagic sediments that have recrystallized to porcellanite and chert as a result of subsidence during diagenesis. Predominance of siliceous microfossils in Unit III is probably indicative of high surface bioproductivity when these sediments deposited near the Equator. The transition from Unit III (cherts) to Unit II (pelagic clays) suggests a significant change in sedimentation rates but this also suggests that sediments were deposited in oligotrophic waters provoking an abrupt decrease in biogenous silica in the sedimentary pile (Plank et al., 2000). Dating of the base of the sediment pile (sediment/chert contact) yielded an age of 134 Ma (Plank et al.,

2000; Ludden et al., 2006). Basement was encountered at 408 mbsf (meters below seafloor) (Figure 1).

The major and trace elements geochemistry in the bulk sediment was measured by ICP-AES and ICP-MS at CRPG (SARM, Nancy, France) and some data were already published in previous papers (Rouxel et al., 2003; Ludden et al., 2006). Radiogenic isotope geochemistry (Pb-Sr-Nd) was also reported for this sedimentary sequence in order to evaluate the composition of the lithogenic component entering the mantle in the "subduction factory" (Hauff et al., 2003). Finally, the first top pelagic clay samples of the sequence as well as some fresh and altered basalts forming the hard substrate of the sequence were previously analyzed for their Ni isotope composition for establishing the Ni isotope composition of the Bulk Silicate Earth (Gueguen et al., 2013).

After chemical purification of Ni through a two-step chromatography columns procedure including first AG1-X8 resin and second Ni-spec resin (Eichrom), Ni isotope compositions were measured by MC-ICP-MS (Neptune Thermo Scientific) at Pôle de Spectrométrie Océan (Ifremer, Brest, France) using a double-spike correction method of the instrumental mass bias (Siebert et al., 2001; Gueguen et al., 2013). Isotope values are reported relatively to the NIST SRM 986 Ni isotope standard according to the usual delta notation (1) :

$$\delta^{60/58}\text{Ni}\ (‰) = (R_{sample}/R_{NIST986} - 1) \times 1000 \qquad (1)$$

where R_{sample} and $R_{NIST986}$ are the $^{60}Ni/^{58}Ni$ ratios of sample and standard NIST SRM 986 respectively. The error associated with sample values is reported as a two-standard error of the mean (2se) calculated with the 50 cycles of measurements during acquisition on the MC-ICP-MS. A sample-standard bracketing method was employed during the analytical protocol, and thus, replicate measurements of NIST SRM 986 allows the calculation of a two-

standard deviation (2s) as the external error of ~0.05 ‰. Analyses of USGS certified reference material BHVO-2 measured along with these samples were already published in Gueguen et al. (2013).

3. Results

Selected elemental ratios and Ni isotope compositions are reported in Table 1 and shown in Figure 2, while representative analyses of major, trace and Rare Earth Elements (REE) of the samples are reported in Table S1 of the **supplementary information**. Elemental geochemistry of the samples shows that along the stratigraphic sequence contents of Ni, Cu, Co and Zn increase with depth and are identical to Mn concentration profile (Figure 2). There is more than a ten-fold increase in Ni/Al ratios from 0.0004 to 0.0054 and Mn/Al varies from 0.012 at 1.4 mbsf to a maximum of 0.155 at 160 mbsf, i.e., a ten-fold increase of Mn/Al ratio (Figure 2 and Table 1). PAAS-normalized (Post-Archean Australian Shale (Taylor and McLennan, 1995)) REE patterns show a slight positive Ce anomaly excepted for the deepest deep-sea clay sample displaying a negative Ce anomaly (Figure 3) and REE enrichment increases with depth of the samples.

The range of $\delta^{60/58}$Ni values along the sedimentary sequence varies from 0.04 to 0.28 ‰ in Unit I and from 0.45 to 1.03 ‰ in Unit II (Figure 2).

4. Discussion

4.1. Evidence for authigenic Mn and associated elements in pelagic clays

Early diagenesis is the predominant process controlling the distribution of metals in oxic sediments, in particular near the sediment/seawater interface. The driving mechanism of these processes is oxidation of organic matter in the upper first centimeters of the sedimentary column during which a redox gradient is formed (Klinkhammer et al., 1982; Bender and Heggie, 1984; Heggie et al., 1986). Although partial enrichment of trace metal in deep-sea pelagic sediments occurs via release of metals contained in the organic matter to porewaters, the presence of a redox gradient combined with low sedimentation rates (~ 1 m/Ma) also allows scavenging of dissolved trace metals from seawater in authigenic phases. Previously established models for the sedimentation history of the sequence at ODP site 1189 indicate that organic supply to the sediment was low and that sedimentation rates varied between 7 and 13 m/Ma for Unit I but were below 2 m/Ma for Unit II (Ludden et al., 2006). Hence, it is unlikely that organic matter decay itself contributed significantly to the increase in transition metals. Several lines of evidence suggest diagenetic Mn recycling through the sedimentary sequence at ODP site 1149. Examination of the concentration profile of dissolved Mn in porewaters indicates that Mn contents decrease from the interface sediment/seawater to ~30 mbsf but increase between 30 and 60 mbsf probably as the result of bacterial reduction of Mn (Plank et al., 2000; Ludden et al., 2006) (Figure 2). This diagenetic sequence has been well identified within pelagic sediments (Heggie et al., 1986), where low sediment rates and oxic conditions favor the enrichment of Mn in surface sediment, which is a typical Mn profile in sediment porewaters. Below 100 mbsf, Mn concentration profile in the sediment shows a clear continuous increase until reaching the base of the pelagic sediment sequence and this profile is mirrored by a decrease in Mn concentrations in sediment porewaters. This suggests that Mn oxidation in porewaters occurs upward (close to the sediment-seawater interface) and in deeper sediments, while in the mid-profile Mn underwent partial reduction. The concentration profile of Ni in the sediment phase is identical to that of Mn consistent with the

fact that Ni is systematically associated with Mn in the diagenetic sequence (Klinkhammer, 1980; Klinkhammer et al., 1982; Heggie et al., 1986). This further validates the assumption that authigenic Mn-oxyhydroxides have a fundamental role in the marine biogeochemical cycling of Ni.

Regardless of any enrichment processes, higher transition metal concentrations in the bulk sediment of pelagic clays compared to the average upper continental crust are generally favored with slow sedimentation rates. Samples of the sedimentary sequence display a flat (shallowest samples) to moderate (deepest samples) positive Ce anomaly, and REE enrichment relatively to PAAS increase with depth of the samples (Figure 3). This is consistent with the fact that samples exhibiting a moderate positive Ce anomaly correspond to samples with very low sedimentation rates < 2 m/Ma (50 meters represent ~90 Ma). Positive Ce anomalies are typically encountered in hydrogenous Fe-Mn deposits forming in deep oceans (De Carlo and McMurtry, 1992) due to the oxidation of Ce^{3+} to Ce^{4+} that forms insoluble CeO_2 at the surface of Fe-oxides minerals which no longer exchanges with ambient seawater, and thus producing Ce enrichment relatively to other REEs (De Baar et al., 1985; German and Elderfield, 1990; Bau, 1999; Bau and Koschinsky, 2009; Bau et al., 2014). However, the deepest sample of the sequence (close to the chert sequence) deviates from this observation because it has a negative Ce anomaly typical to that observed in seawater, and the pattern shows the highest REE enrichment. A plausible hypothesis for this negative Ce anomaly involves the contribution of hydrothermal input of Fe-Mn precipitates. At the time when the sediment deposited, the location of the core could have been affected by inputs from hydrothermal activity emanating from off-axis volcanism (i.e., active seamounts; Ludden et al., 2006). Delivery of significant amount of Mn and Fe by hydrothermal fluids would have promoted precipitation of Mn- and Fe-rich particles in the water column along with incorporation of trace metals like Ni, Cu, Co and Zn and REE from dissolved in seawater. The

later would explain the seawater-like REE pattern with a negative Ce anomaly inherent to seawater (German and Elderfield, 1990; German et al., 1990).

Samples showing the strongest positive Ce anomaly and highest Ni/Al ratios can be considered as the best proxy for the authigenic Ni sink associated with Mn-oxyhydroxides and can be used to estimate the Ni isotope composition of the authigenic Ni sink in modern oceans.

4.2. Ni isotope composition of the authigenic oxic sink in pelagic clays

Previous studies have argued that Ni isotope composition of the authigenic output flux was similar to that of hydrogenetic Fe-Mn crusts and nodules (Gall et al., 2013; Little et al., 2015; Ciscato et al., 2018), in which transition metals are mostly derived from seawater. $\delta^{60/58}$Ni values in nodules range from 0.4 to 1.0 ‰ (Gall et al., 2012; Gall et al., 2013; Gueguen et al., 2013), while hydrogenous Fe-Mn crusts display heavier Ni isotope values from 0.9 and 2.5 ‰ (Gall et al., 2013, Gueguen et al., 2016). Most $\delta^{60/58}$Ni values in Fe-Mn crusts are > 1.0 ‰, which are thus fractionated in heavy Ni isotopes relatively to the Bulk Silicate Earth (i.e., 0.1 ‰; Klaver et al., 2020). The best estimate for Fe-Mn crusts and nodules $\delta^{60/58}$Ni value of ~ 1.6 ‰ (Gall et al., 2013; Gueguen et al., 2016) is similar within uncertainty to the ~1.4 ‰ seawater value (Cameron and Vance, 2014; Takano et al., 2017; Wang et al., 2019; Archer et al., 2020). However, the assumption that the Ni isotope composition of hydrogenetic Fe-Mn deposits is representative of the Ni isotope composition of the authigenic output flux has been questioned by recent studies (Ciscato et al., 2018; Archer et al., 2020; Little et al., 2020). They suggest that the output flux in Fe-Mn crusts and nodules could, in fact, have been overestimated, which would explain the imbalance observed in the marine Ni isotope budget. However, there are few data documenting the Ni isotope

composition of pelagic clays, in particular the composition of the authigenic fraction of deep-sea pelagic clays, which makes estimation of the authigenic output flux difficult. In our study, we calculate an estimate of the pervasive authigenic Fe-Mn oxides sink flux in modern oceanic settings and the associated Ni isotope composition by combining our Al/Ni and Mn/Ni ratios and the $\delta^{60/58}$Ni values measured in buried Fe-Mn oxides in pelagic clay sediment.

A relationship between $\delta^{60/58}$Ni values and 1/Ni and Al/Ni ratios suggests that Ni derives from two sources, one is enriched in isotopically heavy Ni, while the other source is depleted in Ni and has an isotope composition close to the Bulk Silicate Earth (Figure 4). The former can be ascribed to the authigenic end-member, whereas the latter corresponds to the lithogenic end-member. Using the relationship between $\delta^{60/58}$Ni and Al/Ni ratios in Figure 4B and taking a lithogenic end-member with an Al/Ni ratio of ~1700 and a $\delta^{60/58}$Ni value of 0.1 ‰, we inferred a $\delta^{60/58}$Ni value of 1.2 ‰ for the authigenic Ni in pelagic clays. Taking this isotopic value for the authigenic end-member in the plot $\delta^{60/58}$Ni vs. 1/Ni ratio (Figure 4A) is also consistent with the relationship observed in the graph.

We can try to estimate the authigenic Ni based on our previous observations and same reasoning for the $\delta^{60/58}$Ni vs. Mn/Ni plot (Figure 4C). The highest $\delta^{60/58}$Ni values in pelagic clays have Mn/Ni ratios comprised between ~30 and ~60. For comparison, the USGS have compiled data on the chemical composition of Fe-Mn crusts and Mn-nodules from selected areas of the global ocean (Hein et al., 2013). Hydrogenetic Fe-Mn crusts are composed of Fe-Mn oxides layers chemically precipitated from seawater on the flank of marine seamounts. Mn-nodules are Fe-Mn oxides layers precipitated around a nucleus (e.g., shark teeth, rock debris, …) precipitated on the sediment surface in deep abyssal plains. In contrast to hydrogenetic Fe-Mn crusts, the formation of nodules is strongly affected by diagenetic reactions occurring within the sediment. Average Mn/Ni ratios of ~60 and ~70 for Fe-Mn

crusts from the Atlantic and Indian oceans respectively are very similar to the range of Mn/Ni values for North and South Pacific Fe-Mn crusts (i.e., from 50 to 70). In contrast, Mn-nodules yield systematically lower Mn/Ni ratios of about 23-25 for the large nodule fields in the Clarion-Clipperton Zone of the Pacific and the Indian Ocean. The authigenic sink in pelagic clays at site 1149 has a very similar Mn/Ni ratio than the authigenic sink associated with Fe-Mn crusts rather than with Fe-Mn nodules. Therefore, using the Mn/Ni ratio of 60, and a lithogenic end-member with a Mn/Ni ratio of 17 and an isotopic composition of 0.1 ‰, we can draw a relationship within our dataset showing mixing between a lithogenic fraction and an authigenic fraction having a $\delta^{60/58}$Ni value of 1.2 ‰. The relationship between $\delta^{60/58}$Ni values and Mn/Ni ratios is not as clear as for 1/Ni (Figure 4A) and for Al/Ni ratios (Figure 4B) because of a lower number of points from our dataset that plot on the line. In addition, samples with lighter Ni isotope values than the authigenic end-member but high Mn/Ni ratio and which deviate from the relationship between $\delta^{60/58}$Ni and Mn/Ni, are probably due to the presence of hydrothermal precipitates in the base of the sequence (e.g.; Ludden et al., 2006; see also section 4.1). These samples could, therefore, represent the hydrothermal end-member. A possible explanation for lighter Ni isotope values associated with Ni from hydrothermal particles in comparison with seawater Ni and authigenic Ni, is probably the result of isotope fractionation during adsorption of Ni from seawater subsequent to rapid precipitation of Fe- and Mn-oxyhydroxides. This assumption is consistent with results of Gueguen et al. (2016), who showed that post-deposition processes at the base of an Fe-Mn crust produced Fe-Mn oxides with lighter Ni isotopes, and with results of Ni sorption to Mn-oxide phases experiments (Sorensen et al., 2020) showing that sorbed Ni is enriched in lighter Ni isotopes. In addition, Ni isotope fractionation during scavenging onto hydrothermal Fe-oxides particulates was also suggested as a possible explanation for light Ni isotopes relative

to seawater (-0.8 ‰) found in metalliferous sediments from the MANOP site M in the East Pacific (Little et al., 2020).

To compare with our observations, the Ni isotope composition of the authigenic fraction can also be estimated using a mass balance equation (2a) including an estimate of the detrital fraction using the Ni/Al ratio of the Upper Continental Crust (UCC) of 0.0006 (Rudnick and Gao, 2014) and the Ni isotope composition of the Bulk Silicate Earth (i.e., 0.1 ‰; Klaver et al., 2020).

$$\delta^{60/58}Ni_{auth} = (\delta^{60/58}Ni_{bulk\ sed} - ((1-f_{auth}) \times \delta^{60/58}Ni_{det}))/f_{auth} \quad (2a)$$

$$f_{auth} = ([Ni]_{bulk\ sed} - ([Al]_{bulk\ sed} \times [Ni]_{det}/[Al]_{det}))/[Ni]_{bulk\ sed} \quad (2b)$$

Subscript 'auth' stands for the authigenic fraction; 'bulk sed' is for the bulk pelagic clay sediment samples from Unit II; and 'det' corresponds to the detrital fraction (i.e., average detrital Ni/Al ratio for the UCC of 0.0006 and $\delta^{60/58}$Ni value of the BSE of 0.1 ‰). The authigenic Ni isotope composition derived from equations (2a) and (2b) using the three samples from Unit II (the three brown pelagic clays samples) yields an average value of ~ 1.0 ±0.3 ‰, which is similar, within uncertainty, to the value of 1.2 ‰ we have determined in this study using trace metal ratios and Ni isotope values in pelagic clays.

In summary, the negative relationship between Ni isotope values and Al/Ni ratios (or inverse Ni concentration) is likely indicative of mixing between a close to zero $\delta^{60/58}$Ni value (~0.1 ‰) end-member and a positive end-member of 1.2 ‰ (Figure 4). High Al/Ni and close to zero $\delta^{60/58}$Ni values (~0.1 ‰) are consistent with the high detrital component of pelagic clays. The heavy Ni isotope composition, metal-rich and low Al/Ni ratio end-member are consistent with the composition of authigenic Mn-oxyhydroxides. Our results show that in comparison to the average $\delta^{60/58}$Ni value of about 1.6 ‰ reported in Fe-Mn crusts, our estimated $\delta^{60/58}$Ni value for the authigenic Ni sink in pelagic clays of 1.2 ‰ is lighter by ~ 0.4

‰ than Fe-Mn crusts and nodules but is similar to the best estimate for authigenic Ni in organic-rich sediments (i.e., 1.2 ‰ in Peru margin sediments; Ciscato et al., 2018).

4.3. Implications for the global modern marine Ni budget and its isotopes

A review of the source and sink fluxes for Ni including results from mass balance calculations of this study is given in Table 2. Nickel is essentially delivered to the oceans by continental runoff with a flux of 5.11 x 10^8 mol/yr (Gaillardet et al., 2003; Chester and Jickells, 2012; Cameron and Vance, 2014; Little et al., 2015; Ciscato et al., 2018). Nickel isotope composition of rivers yield a discharge and concentrations-weighted average value of 0.8 ‰ (Cameron and Vance, 2014). Additional input fluxes include an atmospheric flux of ~0.07 x 10^8 mol/yr (Rehkämper and Nielsen, 2004; Desboeufs et al., 2005; Little et al., 2015) and a hydrothermal flux of 0.14 x 10^8 mol/yr (Elderfield and Schultz, 1996; Douville et al., 2002; Wheat et al., 2002; German and Von Damm, 2003), for which we assume a Ni isotope composition close to the Bulk Silicate Earth of 0.1 ‰.

Elderfield and Schultz (1996) estimated a global hydrothermal flux of Mn between 1.1 to 3.4 x 10^{10} mol/yr, higher than the riverine Mn flux of 0.5 x 10^{10} mol/yr (Elderfield and Schultz, 1996; German and Von Damm, 2003). At steady-state conditions and assuming that input fluxes of Ni and Mn remained constant over the last 100 Ma, one can combine the input Mn flux with the Mn/Ni ratio of 60 estimated for the authigenic Mn sink in pelagic sediment to calculate an average oxic Ni sink of 3.58 x 10^8 mol/yr. Combining this output flux with the Ni output flux in Fe-Mn crusts and nodules of 5.11 x 10^8 mol/yr (Gall et al., 2013), the Ni sink in organic matter-rich sediments of 1.60 x 10^8 mol/yr (Ciscato et al., 2018), and the output fluxes in euxinic sediments and carbonate sediments respectively of 0.15 x 10^8 mol/yr

and 0.14 x 10^8 mol/yr (Ciscato et al., 2018), one can see that input fluxes do not balance the output fluxes.

Assuming that steady state conditions prevail in the oceans, one can use a mass balance model (3) to calculate the Ni isotope compositions of the input and output fluxes and their magnitude :

$$\sum F_i^{in} . \delta^{60/58}Ni_i^{in} = \sum F_i^{out} . \delta^{60/58}Ni_i^{out} \quad (3)$$

Where F_i^{in} and F_i^{out} are the Ni input and output fluxes respectively and $\delta^{60/58}Ni_i^{in}$ and $\delta^{60/58}Ni_i^{out}$ are their respective Ni isotope composition. Using equation (4) we can calculate the Ni isotope composition of the missing flux :

$$\sum F_i^{out} . \delta^{60/58}Ni_i^{out} = \sum F_i^{in} . \delta^{60/58}Ni_i^{in} + F^{in}_{miss} . \delta^{60/58}Ni^{in}_{miss} \quad (4)$$

Using these mass balance equations, we calculate that with a diagenetic input flux (or benthic flux) of 3.7 x 10^8 mol/yr, mass balance at steady-state conditions is preserved. Calculations indicate that the Ni isotope composition of the diagenetic input flux would be 2.85 ‰ which is highly fractionated from seawater. The isotopic value is very similar to the value recently calculated (~ 3 ‰) for the benthic flux by Little et al. (2020), although we calculated a different value for the magnitude of the input flux.

5. Summary

Quantification of the global marine Ni budget both in terms of fluxes and isotope composition to establish a model of mass balance is a critical step in order to use Ni isotope composition archived in modern marine sediments as a proxy of seawater. Pervasive

authigenic Mn-oxides in pelagic clays represents the major oxic sink for Ni in modern oceans and, thus, this reservoir should have a strong control on the isotope composition of modern seawater. Ferromanganese crusts and nodules were often employed to estimate the Ni isotope composition of the authigenic sink which is not necessarily accurate.

We targeted a sequence of deep-sea pelagic clays deposited on the old western Pacific oceanic crust in order to evaluate the global authigenic output flux of Ni in modern oceans and its Ni isotope composition. We calculated that a flux of 3.58 x 10^8 mol/yr of Ni is removed in authigenic Mn-oxides with an average Ni isotope composition of ~1.2 ‰. This isotopic value is ~ 0.4 ‰ lighter than the average $\delta^{60/58}$Ni value previously determined for Fe-Mn crusts and nodules. To balance the Ni marine budget, we calculate a diagenetic flux of 3.7 x 10^8 mol/yr with an isotopic composition of ~2.9 ‰

Acknowledgments :

We thank Marie-Laure Rouget, Yoan Germain and Emmanuel Ponzevera for technical assistance in the clean lab, for ICP-MS and MC-ICP-MS analyses. We thank the two anonymous reviewers for thoughtful corrections and suggestions that significantly improved the manuscript.

Figure captions :

Figure 1: Map of the drilling core position and stratigraphic log of site 1149 (map from Ludden et al. (2006) and stratigraphic log reproduced from Plank et al. (2000)).

Figure 2: Stratigraphic log of the sediment sequence including samples investigated in this study, and depth profiles (mbsf, meters below seafloor) of geochemical (Mn, Ni, Al,

Cu+Co+Zn, Ni/Al and Mn/Al) and Ni isotope composition of sediments. The right panel shows a depth profile of dissolved Mn (µM/L) in sediment porewaters (plot reproduced from Ludden et al. 2006). The increase in Ni concentration and Mn/Al ratio in the sediment is concomitant to a decrease in Mn concentration in sediment porewaters possibly suggesting precipitation of Mn-oxyhydroxides and scavenging of trace metals. Increase in Ni isotope composition from ~ 0.0 ‰ to ~ 1.2 ‰ is consistent with scavenging of Ni from porewaters in authigenic Mn-oxyhydroxides phases.

Figure 3: Rare Earth Elements patterns normalized to PAAS (Post-Archean Australian Shale (Taylor and McLennan, 1995)) of pelagic clays. Symbols stands for depth (mbsf) of samples in the stratigraphic sequence.

Figure 4: Plots showing Ni isotope composition of pelagic clays versus inverse Ni concentration (A), versus Al/Ni ratio (B) and versus Mn/Ni ratio (C). The assumed authigenic and lithogenic end-members are represented on the three plots A, B and C. The lithogenic end-member is defined with the concentration values for the Upper Continental Crust (UCC; Rudnick and Gao, 2014) and the Ni isotope composition of the Bulk Silicate Earth (BSE; Klaver et al., 2020). Intersection of the linear relationship defined by samples between these two end-members and the y-axis is the assumed Ni isotope composition of the authigenic Ni in pelagic sediments which can be determined at 1.2 ‰. Using this value in plot C, we can determine a Mn/Ni ratio for the authigenic end-member of pelagic sediments of 60. Additional possible hydrothermal end-member is also shown in plot C.

TABLE CAPTIONS

Table 1: Ni isotope composition (‰), Ni concentration (µg/g) and elemental ratios (µg/µg) of pelagic clays from ODP site 1149.

Sample name	Depth (mbsf)	Description of samples	$\delta^{60/58}$Ni (‰)	2se	Ni	Mn/Al	Al/Ni	Mn/
1149A-01H1,140	1.4	Ash and silica-bearing clay	0.04	0.04	33.2	0.012	2409	28
1149A-04H2,140	26.1	Clay	0.02	0.03	54.9	0.012	1401	17
1149A-05H5,140	40.1	Clay	0.15	0.03	53.2	0.010	1499	15
1149A-07H4,140	57.6	Ash-bearing siliceous silty clay	0.09	0.03	31.9	0.027	2280	61
1149A-09H3,140	75.1	Ash-bearing siliceous silty clay	0.19	0.03	39.8	0.029	2058	60
1149A-10H3,140	84.6	Ash-bearing siliceous silty clay	0.15	0.03	46.3	0.057	1816	10
1149A-12H3,140	103.6	Ash-rich clay	0.28	0.03	55.7	0.050	1452	73
1149A-16H3,140	141.6	Clay	0.45	0.04	71.9	0.073	1136	83
1149A-18H3,140	160.4	Pelagic clay	1.03	0.03	276.0	0.155	320	50
1149A-20X1,140	171.2	Silt-bearing clay	0.77	0.03	428.9	0.154	184	28

Table 2: Output and input fluxes of Ni (in 10^8 mol/yr) and Ni isotopes (‰) in modern oceans.

	Input fluxes (10^8 mol/yr)	**$\delta^{60/58}$Ni (‰)**	**Reference**
Rivers	5.11	0.80	1, 2
Hydrothermal vents	0.14	0.10	This study
Atmospheric dusts	0.07	0.10	3
Diagenetic/benthic	3.70	*2.85**	4 and this study
	Output fluxes (10^8 mol/yr)		
Fe-Mn deposits	5.11	1.50	5
Authigenic oxic sediments	3.58	1.20	This study
Organic-rich sediments - Anoxic	1.60	1.19	6
Carbonate sediments	0.14	1.29	6
Euxinic sediments	0.15	0.45	6

1 Cameron et al. (2014); 2 Vance et al. (2016); 3 Little et al. (2015); 4 Little et al. (2020); 5 Gall et al. (2013); 6 Ciscato
*Value in italic determined by mass balance calculations.

.

REFERENCES CITED

Albarède, F., Beard, B., 2004. Analytical Methods for Non-Traditional Isotopes. Reviews in Mineralogy and Geochemistry, 55(1): 113-152.

Anbar, A.D., Rouxel, O., 2007. Metal stable isotopes in paleoceanography. Annual Review of Earth and Planetary Sciences, 35: 717-746.

Archer, C., Vance, D., 2008. The isotopic signature of the global riverine molybdenum flux and anoxia in the ancient oceans. Nature Geoscience, 1(9): 597-600.

Archer, C., Vance, D., Milne, A., Lohan, M.C., 2020. The oceanic biogeochemistry of nickel and its isotopes: New data from the South Atlantic and the Southern Ocean biogeochemical divide. Earth and Planetary Science Letters, 535: 116118.

Bartolini, A., Larson, R.L., 2001. Pacific microplate and the Pangea supercontinent in the Early to Middle Jurassic. Geology, 29(8): 735-738.

Bau, M., 1999. Scavenging of dissolved yttrium and rare earths by precipitating iron oxyhydroxide: experimental evidence for Ce oxidation, Y-Ho fractionation, and lanthanide tetrad effect. Geochimica Et Cosmochimica Acta, 63(1): 67-77.

Bau, M., Koschinsky, A., 2009. Oxidative scavenging of cerium on hydrous Fe oxide: Evidence from the distribution of rare earth elements and yttrium between Fe oxides and Mn oxides in hydrogenetic ferromanganese crusts. Geochemical Journal, 43(1): 37-47.

Bau, M., Schmidt, K., Koschinsky, A., Hein, J., Kuhn, T., Usui, A., 2014. Discriminating between different genetic types of marine ferro-manganese crusts and nodules based on rare earth elements and yttrium. Chemical Geology, 381(0): 1-9.

Bender, M.L., Heggie, D.T., 1984. Fate of organic carbon reaching the deep sea floor: a status report. Geochimica et Cosmochimica Acta, 48(5): 977-986.

Boström, K., Peterson, M.N.A., 1966. Precipitates from hydrothermal exhalations on the East Pacific rise. Economic Geology, 61(7): 1258-1265.

Boström, K., Peterson, M.N.A., Joensuu, O., Fisher, D.E., 1969. Aluminum-poor ferromanganoan sediments on active oceanic ridges. Journal of Geophysical Research, 74(12): 3261-3270.

Cameron, V., Vance, D., 2014. Heavy nickel isotope compositions in rivers and the oceans. Geochimica Et Cosmochimica Acta, 128(0): 195-211.

Chester, R., Jickells, T., 2012. Marine Geochemistry, Marine Geochemistry. John Wiley & Sons, Ltd.

Ciscato, E.R., Bontognali, T.R.R., Vance, D., 2018. Nickel and its isotopes in organic-rich sediments: implications for oceanic budgets and a potential record of ancient seawater. Earth and Planetary Science Letters, 494: 239-250.

De Baar, H.J.W., Bacon, M.P., Brewer, P.G., Bruland, K.W., 1985. Rare Earth elements in the Pacific and Atlantic Oceans. Geochimica Et Cosmochimica Acta, 49(9): 1943-1959.

De Carlo, E.H., McMurtry, G.M., 1992. Rare-earth element geochemistry of ferromanganese crusts from the Hawaiian Archipelago, central Pacific. Chemical Geology, 95(3–4): 235-250.

Desboeufs, K.V., Sofikitis, A., Losno, R., Colin, J.L., Ausset, P., 2005. Dissolution and solubility of trace metals from natural and anthropogenic aerosol particulate matter. Chemosphere, 58(2): 195-203.

Douville, E., Charlou, J.L., Oelkers, E.H., Bienvenu, P., Colon, C.F.J., Donval, J.P., Fouquet, Y., Prieur, D., Appriou, P., 2002. The rainbow vent fluids (36 degrees 14 ' N, MAR): the influence of ultramafic rocks and phase separation on trace metal content in Mid-Atlantic Ridge hydrothermal fluids. Chemical Geology, 184(1-2): 37-48.

Elderfield, H., Schultz, A., 1996. Mid-ocean ridge hydrothermal fluxes and the chemical composition of the ocean. Annual Review of Earth and Planetary Sciences, 24: 191-224.

Gaillardet, J., Viers, J., Dupré, B., 2003. Trace Elements in River Waters. In: Editors-in-Chief: Heinrich, D.H., Karl, K.T. (Eds.), Treatise on Geochemistry. Pergamon, Oxford, pp. 225-272.

Gall, L., Williams, H., Siebert, C., Halliday, A., 2012. Determination of mass-dependent variations in nickel isotope compositions using double spiking and MC-ICPMS. Journal of Analytical Atomic Spectrometry, 27(1): 137-145.

Gall, L., Williams, H.M., Siebert, C., Halliday, A.N., Herrington, R.J., Hein, J.R., 2013. Nickel isotopic compositions of ferromanganese crusts and the constancy of deep ocean inputs and continental weathering effects over the Cenozoic. Earth and Planetary Science Letters, 375(0): 148-155.

German, C.R., Elderfield, H., 1990. Application of the Ce Anomaly as a Paleoredox Indicator: The Ground Rules. Paleoceanography, 5(5): 823-833.

German, C.R., Klinkhammer, G.P., Edmond, J.M., Mitra, A., Elderfield, H., 1990. Hydrothermal scavenging of rare earth elements in the ocean. Nature, 345(6275): 516-518.

German, C.R., Von Damm, K.L., 2003. Hydrothermal Processes. In: Editors-in-Chief: Heinrich, D.H., Karl, K.T. (Eds.), Treatise on Geochemistry. Pergamon, Oxford, pp. 181-222.

Glasby, G.P., 1991. Mineralogy, geochemistry, and origin of Pacific red clays: a review. New Zealand Journal of Geology and Geophysics, 34(2): 167-176.

Goldberg, E.D., Arrhenius, G.O.S., 1958. Chemistry of Pacific pelagic sediments. Geochimica et Cosmochimica Acta, 13(2–3): 153-212.

Goldberg, T., Archer, C., Vance, D., Poulton, S.W., 2009. Mo isotope fractionation during adsorption to Fe (oxyhydr)oxides. Geochimica et Cosmochimica Acta, 73(21): 6502-6516.

Gueguen, B., Rouxel, O., Ponzevera, E., Bekker, A., Fouquet, Y., 2013. Nickel Isotope Variations in Terrestrial Silicate Rocks and Geological Reference Materials Measured by MC-ICP-MS. Geostandards and Geoanalytical Research, 37(3): 297-317.

Gueguen, B., Rouxel, O., Rouget, M.-L., Bollinger, C., Ponzevera, E., Germain, Y., Fouquet, Y., 2016. Comparative geochemistry of four ferromanganese crusts from the Pacific Ocean and significance for the use of Ni isotopes as paleoceanographic tracers. Geochimica et Cosmochimica Acta, 189: 214-235.

Hannington, M.D., 2013. The role of black smokers in the Cu mass balance of the oceanic crust. Earth and Planetary Science Letters, 374: 215-226.

Hauff, F., Hoernle, K., Schmidt, A., 2003. Sr-Nd-Pb composition of Mesozoic Pacific oceanic crust (Site 1149 and 801, ODP Leg 185): Implications for alteration of ocean crust and the input into the Izu-Bonin-Mariana subduction system. Geochemistry, Geophysics, Geosystems, 4(8): 8913.

Heggie, D., Kahn, D., Fischer, K., 1986. Trace metals in metalliferous sediments, MANOP Site M: interfacial pore water profiles. Earth and Planetary Science Letters, 80(1–2): 106-116.

Hein, J.R., Mizell, K., Koschinsky, A., Conrad, T.A., 2013. Deep-ocean mineral deposits as a source of critical metals for high- and green-technology applications: Comparison with land-based resources. Ore Geology Reviews, 51(0): 1-14.

Kadko, D., 1985. Late Cenozoic sedimentation and metal deposition in the North Pacific. Geochimica et Cosmochimica Acta, 49(3): 651-661.

Klaver, M., Ionov, D.A., Takazawa, E., Elliott, T., 2020. The non-chondritic Ni isotope composition of Earth's mantle. Geochimica et Cosmochimica Acta, 268: 405-421.

Klinkhammer, G., Heggie, D.T., Graham, D.W., 1982. Metal diagenesis in oxic marine-sediments. Earth and Planetary Science Letters, 61(2): 211-219.

Klinkhammer, G.P., 1980. Early diagenesis in sediments from the eastern equatorial Pacific, II. Pore water metal results. Earth and Planetary Science Letters, 49(1): 81-101.

Krishnaswami, S., 1976. Authigenic transition elements in Pacific pelagic clays. Geochimica Et Cosmochimica Acta, 40(4): 425-434.

Kyte, F.T., Leinen, M., Ross Heath, G., Zhou, L., 1993. Cenozoic sedimentation history of the central North Pacific: Inferences from the elemental geochemistry of core LL44-GPC3. Geochimica et Cosmochimica Acta, 57(8): 1719-1740.

Leinen, M., 1987. The origin of paleochemical signatures in North Pacific pelagic clays: Partitioning experiments. Geochimica et Cosmochimica Acta, 51(2): 305-319.

Little, S.H., Archer, C., McManus, J., Najorka, J., Wegorzewski, A.V., Vance, D., 2020. Towards balancing the oceanic Ni budget. Earth and Planetary Science Letters, 547: 116461.

Little, S.H., Vance, D., Lyons, T.W., McManus, J., 2015. Controls on trace metal authigenic enrichment in reducing sediments: Insights from modern oxygen-deficient settings. American Journal of Science, 315(2): 77-119.

Little, S.H., Vance, D., Walker-Brown, C., Landing, W.M., 2014. The oceanic mass balance of copper and zinc isotopes, investigated by analysis of their inputs, and outputs to ferromanganese oxide sediments. Geochimica et Cosmochimica Acta, 125(0): 673-693.

Ludden, J.N., Plank, T., Larson, R., Escutia, C., 2006. Leg 185 Synthesis: Sampling the Oldest Crust in the Ocean Basins to Understand Earth's Geodynamic and Geochemical Fluxes Proceedings of the Integrated Ocean Drilling Program, Scientific Results, 185.

Nägler, T.F., Neubert, N., Böttcher, M.E., Dellwig, O., Schnetger, B., 2011. Molybdenum isotope fractionation in pelagic euxinia: Evidence from the modern Black and Baltic Seas. Chemical Geology, 289(1–2): 1-11.

Plank, T., Ludden, J.N., Escutia C., Party, S.S., 2000. Site 1149. Proceedings of the Ocean Drilling Program, Initial Reports, 185.

Rehkämper, M., Nielsen, S.G., 2004. The mass balance of dissolved thallium in the oceans. Marine Chemistry, 85(3-4): 125-139.

Reinhard, C.T., Planavsky, N.J., Robbins, L.J., Partin, C.A., Gill, B.C., Lalonde, S.V., Bekker, A., Konhauser, K.O., Lyons, T.W., 2013. Proterozoic ocean redox and biogeochemical stasis. Proceedings of the National Academy of Sciences of the United States of America, 110(14): 5357-62.

Rouxel, O., Dobbek, N., Ludden, J., Fouquet, Y., 2003. Iron isotope fractionation during oceanic crust alteration. Chemical Geology, 202(1-2): 155-182.

Rudnick, R.L., Gao, S., 2014. Composition of the Continental Crust. In: Holland, H.D., Turekian, K.K. (Eds.), Treatise on Geochemistry (Second Edition). Elsevier, Oxford, pp. 1-51.

Schauble, E.A., 2004. Applying Stable Isotope Fractionation Theory to New Systems. Reviews in Mineralogy and Geochemistry, 55(1): 65-111.

Scott, C., Lyons, T.W., 2012. Contrasting molybdenum cycling and isotopic properties in euxinic versus non-euxinic sediments and sedimentary rocks: Refining the paleoproxies. Chemical Geology, 324–325(0): 19-27.

Siebert, C., Nagler, T.F., Kramers, J.D., 2001. Determination of molybdenum isotope fractionation by double-spike multicollector inductively coupled plasma mass spectrometry. Geochemistry Geophysics Geosystems, 2: 1032.

Sorensen, J.V., Gueguen, B., Stewart, B.D., Peña, J., Rouxel, O., Toner, B.M., 2020. Large nickel isotope fractionation caused by surface complexation reactions with hexagonal birnessite. Chemical Geology, 537: 119481.

Takano, S., Tanimizu, M., Hirata, T., Shin, K.-C., Fukami, Y., Suzuki, K., Sohrin, Y., 2017. A simple and rapid method for isotopic analysis of nickel, copper, and zinc in seawater using chelating extraction and anion exchange. Analytica Chimica Acta, 967: 1-11.

Taylor, S.R., McLennan, S.M., 1995. The geochemical evolution of the continental crust. Reviews of Geophysics, 33(2): 241-265.

Vance, D., Little, S.H., Archer, C., Cameron, V., Andersen, M.B., Rijkenberg, M.J.A., Lyons, T.W., 2016. The oceanic budgets of nickel and zinc isotopes: the importance of sulfidic environments as illustrated by the Black Sea. Philosophical Transactions of the Royal Society A: Mathematical, Physical and Engineering Sciences, 374(2081).

Wang, R.M., Archer, C., Bowie, A.R., Vance, D., 2019. Zinc and nickel isotopes in seawater from the Indian Sector of the Southern Ocean: The impact of natural iron fertilization versus Southern Ocean hydrography and biogeochemistry. Chemical Geology, 511: 452-464.

Wheat, C.G., Mottl, M.J., Rudnicki, M., 2002. Trace element and REE composition of a low-temperature ridge-flank hydrothermal spring. Geochimica Et Cosmochimica Acta, 66(21): 3693-3705.

Wille, M., Nebel, O., Van Kranendonk, M.J., Schoenberg, R., Kleinhanns, I.C., Ellwood, M.J., 2013. Mo–Cr isotope evidence for a reducing Archean atmosphere in 3.46–2.76 Ga black shales from the Pilbara, Western Australia. Chemical Geology, 340(0): 68-76.

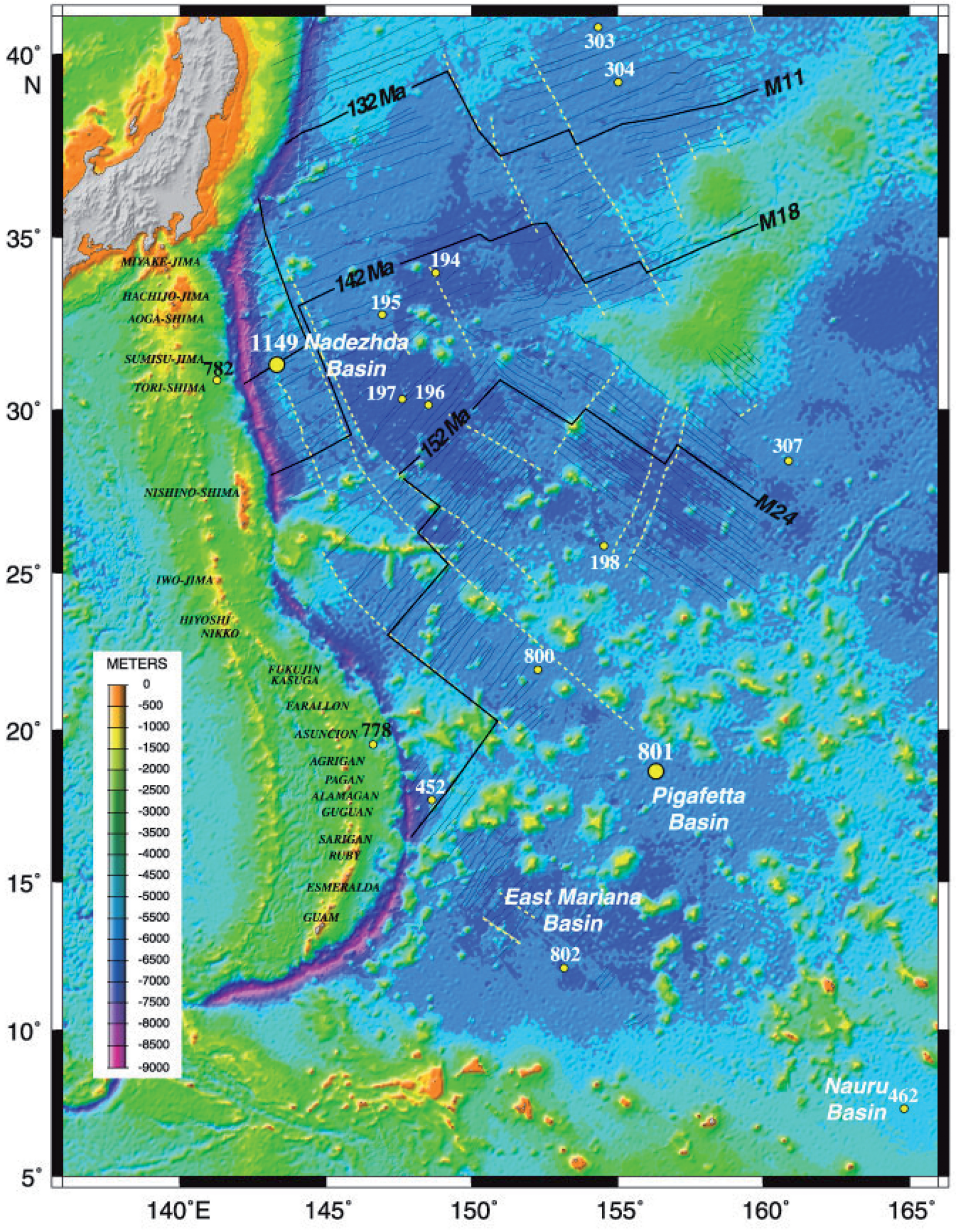

Stratigraphic log of site 1149

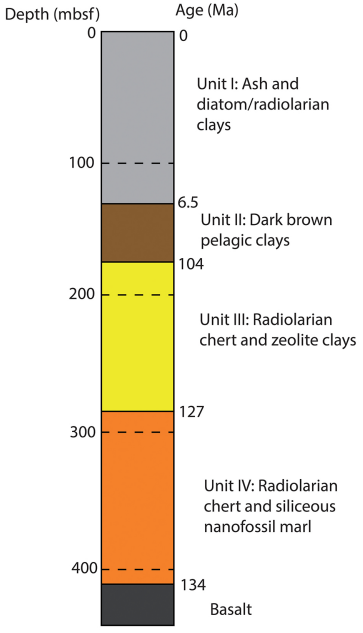

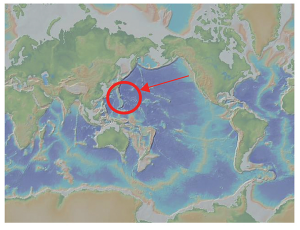

Figure 1

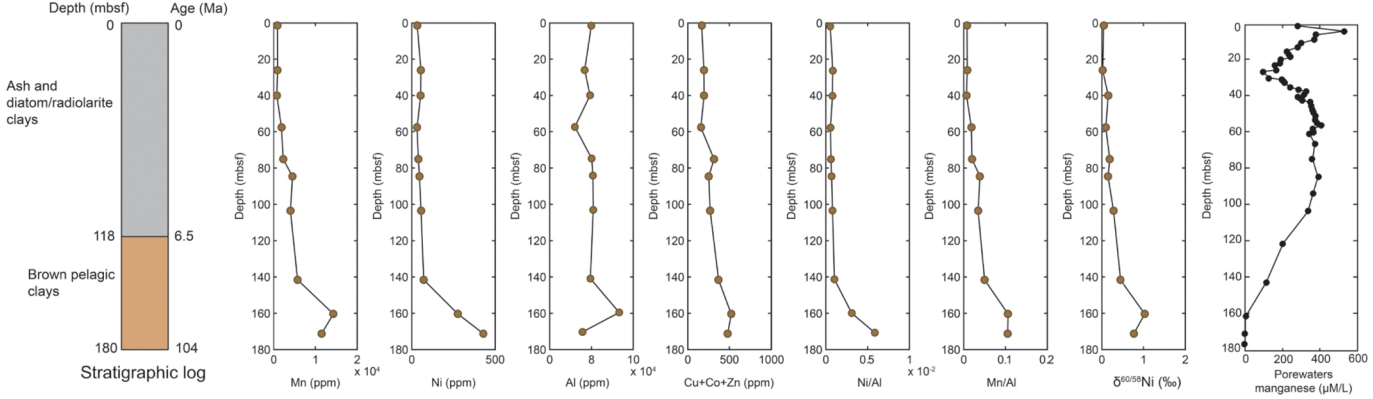
Depth (mbsf)
Age (Ma)
0
0
Ash and diatom/radiolarite clays
118
6.5
Brown pelagic clays
180
104
Stratigraphic log
Depth (mbsf)
Mn (ppm)
x 10^4
Ni (ppm)
Al (ppm)
x 10^4
Cu+Co+Zn (ppm)
Ni/Al
x 10^-2
Mn/Al
δ60/58Ni (‰)
Porewaters manganese (μM/L)

Figure 2

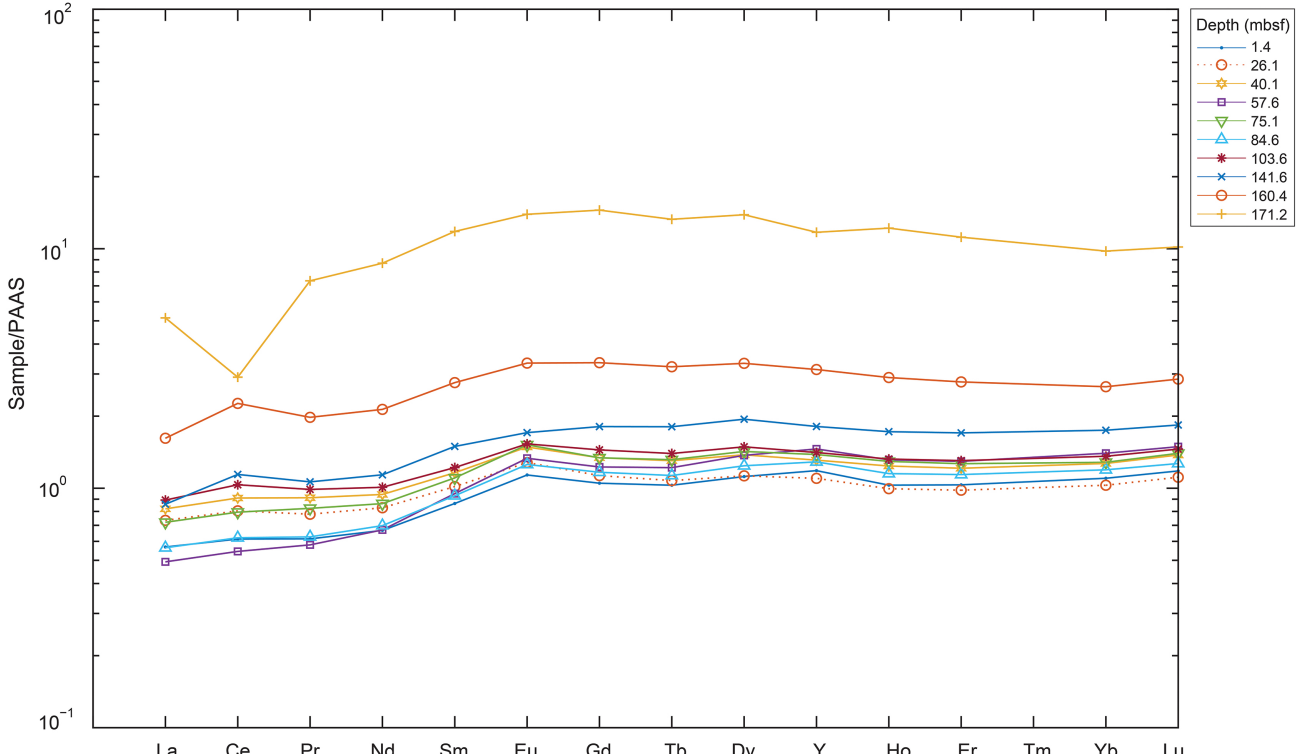
Depth (mbsf)
1.4
26.1
40.1
57.6
75.1
84.6
103.6
141.6
160.4
171.2
Sample/PAAS
10^2
10^1
10^0
10^{-1}
La
Ce
Pr
Nd
Sm
Eu
Gd
Tb
Dy
Y
Ho
Er
Tm
Yb
Lu

Figure 3

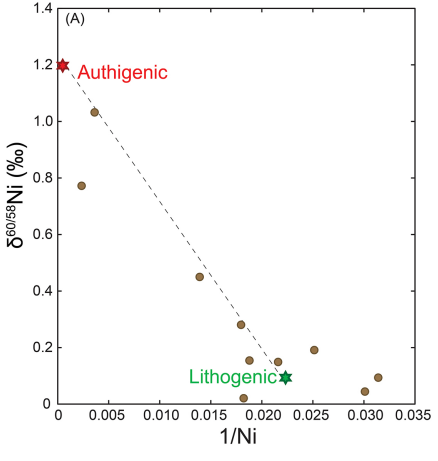
(A)
Authigenic
Lithogenic
δ60/58Ni (‰)
1/Ni
0
0.2
0.4
0.6
0.8
1.0
1.2
1.4
0.005
0.010
0.015
0.020
0.025
0.030
0.035

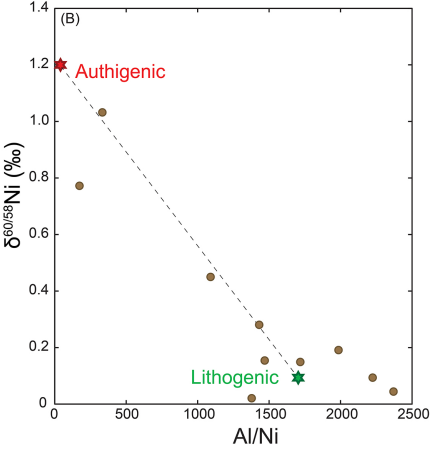
(B)
Authigenic
Lithogenic
δ60/58Ni (‰)
Al/Ni
0
0.2
0.4
0.6
0.8
1.0
1.2
1.4
500
1000
1500
2000
2500

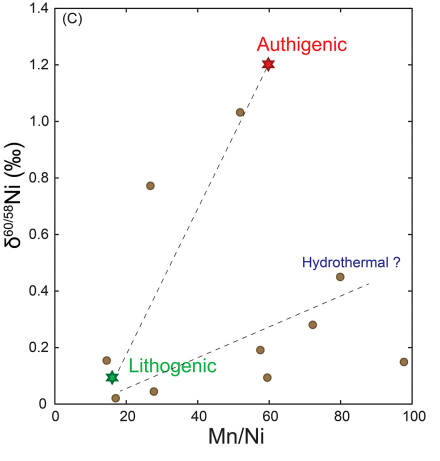
(C)
Authigenic
Hydrothermal ?
Lithogenic
δ60/58Ni (‰)
Mn/Ni
0
0.2
0.4
0.6
0.8
1.0
1.2
1.4
20
40
60
80
100

Figure 4